—NOTE—

Basic Assessment of Diagnosis by MDCT in Horses

Naoki SASAKI[1*], Takuya KIKUCHI[1], Kazutaka YAMADA[1], Tohru HIGUCHI[2], Motoyoshi SATO[1] and Haruo YAMADA[1]

[1]Department of Clinical Veterinary Science, Obihiro University of Agriculture & Veterinary Medicine, Inada-town, Obihiro-city, Hokkaido 080-8555, and [2]Animal Clinic Center, Agricultural Mutual Relief Association, Higashihorai 200, Mitsuishi, Hokkaido 059-3105, Japan

In this equine study, we used an MDCT unit and a trestle for large animals to assess the utility of MDCT in the diagnosis locomotor system disorders and problems in the head and spine. We used a mature thoroughbred horse under general anesthesia and 5 specimens. For specimens, MDCT images were compared with other images taken by a computed radiography X-ray unit. In the live horse, use of the trestle for large animals enabled scanning under general anesthesia. In specimens, MDCT created 3D images of the fractured lesions and evaluation of multiple cross-sectional and sagittal images was possible. Further, multiple sagittal images and virtual endoscopic images revealed details of a spinal canal stenosis in the swayback case. These results indicate that MDCT is useful for diagnosing and viewing details of cases that conventional X-ray images do not capture.

Key words: *equine, locomotor system disorders, MDCT, 3D image analysis*

J. Equine Sci.
Vol. 18, No. 1
pp. 33–38, 2007

In horses, locomotor system disorders and problems in the head and spine (such as limb fractures, sinusitis, and wobbler syndrome) are common, and their diagnosis is considered important for determining prognosis [1, 5–7]. Conventionally, these problems in horses have been diagnosed mainly by plain X-ray and endoscopy [2, 8]. However, in some instances, such as multiple fractures and abnormality in the cervical vertebrae, interpretation of two-dimensional (2D) images can be difficult, and use of multidetector-row computed tomography (MDCT) in diagnosing such problems has been discussed [3, 11]. MDCT is different from conventional single-slice CT, since an X-ray tube that consists of multiple detectors continuously rotates and it has a table which also continuously moves. With these features, MDCT can instantly create accurate cross-sectional images as well as 3D images. In this equine study, we used an MDCT unit and a trestle for large animals to assess its ability to diagnose locomotor system disorders and problems in the head and spine.

We used a mature thoroughbred horse (500 kg, aged 13 years, female) under anesthesia and 5 specimens (overgrown hoof, comminuted fracture of the proximal phalanx, multiple fracture of the carpal bone, normal head, and vertebral column of a swayback) collected from horses of poor prognosis diagnosed by farms in the Hidaka area and euthanized by Hidaka NOSAI Live Animal Clinic. The normal head came from a horse of poor prognosis that was diagnozed with a bent limb (Table 1). CT images were taken by a MDCT unit (Asterion super 4, Toshiba, Japan), which had four rows of detectors. For general anesthesia of the live horse, following sedation with 0.004 mg/kg of medetomidine hydrochloride, 2 mg/kg ketamine hydrochloride and 0.03 mg/kg diazepam were administered and the horse was laid on its side. Then, 500 m*l* of 5% GGE rapid intravenous infusion was administered, and the animal was secured on the trestle (Fig. 1). General anesthesia was maintained with a triple drip containing 5% GGE at 4 m*l*/kg/hr. The MDCT table was connected to the trestle for large animals (180 cm × 320 cm, maximum load: 600 kg), and interlocked the trestle when the table moved horizontally. The top table of the trestle was made movable, so that images in both recumbency and

This article was accepted December 4, 2006
*Corresponding author. e-mail: naoki@obihiro.ac.jp

Table 1. Materials used in the present study

disease	part	age (year)	sex	weight(kg)
1) general aneathesia	foot	13	female	500
2) specimens				
overgrowth hoof	hoof	23	mare	500
comminuted fracture	proximal phalanx	4	mare	500
multiple fracture	carpal joint	8	female	500
normal head	nasal meatus	1 month	mare	100
wobbler syndrome	cervical vertebrae	1	mare	300

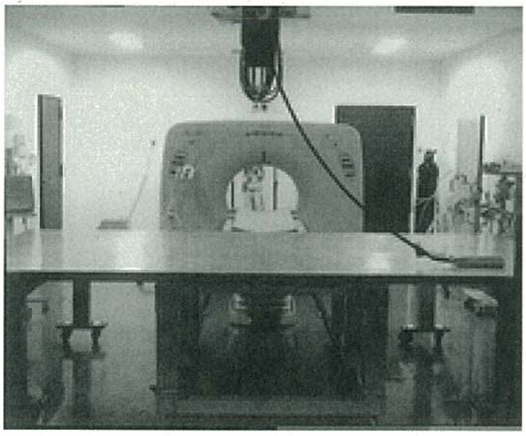

Fig. 1. The trestle for large animals and the MDCT unit. Scanning of large animals was possible by securing animals on the trestle connected to a table. The maximum load for this trestle is 600 kg, and it moves with the table while scanning.

Fig. 2. A 3D image captured by MDCT showing the lateral bottom of the forelimb of the live horse. Imaging conditions: 135 kV, 150 mA, 1 mm slice thickness.

supine positions could be captured. The live horse was secured on the trestle for a large animal, and the limb was secured on the MDCT table. When taking the MDCT images, the MDCT table and the trestle for a large animal were synchronize and the animal moved. The left forelimb and left hindlimb were scanned by MDCT at 135 kV, 150 mA, and 1-mm slice thickness, and 2D and 3D images were constructed using software that performs high-precision, high-speed 3D image analysis (Virtual Place Advance, AZE, Japan). For specimens, we compared images taken by a computed radiography (CR) X-ray unit with a portable X-ray source (70 kV, 10 mA) and those taken by the MDCT unit.

For the live horse, use of the trestle for large animals enabled scanning under general anesthesia. Bone structures in joints and structures in deep parts of the hoof were clearly shown. Due to a technical difficulty associated with the trestle, the images we captured were limited to the carpal joint, hock and the lower parts of the limbs (Fig. 2).

For the specimens, 3D reconstructed images of the hoof showed detailed structures of the digits 1, 2, and 3. When compared with X-ray images, 3D images provided the detailed shape of the navicular bone in the deep part of the hoof (Figs. 3, 4). X-ray images of the comminuted fracture of the proximal phalanx showed overlapping fracture lines and unclear lesions, and we needed to capture images from various angles to understand the details (Fig. 5). However, 3D images constructed by MDCT helped us to understand complicated fracture lines associated with the comminuted fracture (Fig. 6). X-ray images of the carpal bone fracture visualized the presence of the multiple fracture although they were unclear (Fig. 7). Since MDCT diagnosis involves various sagittal and cross-sectional views, detailed diagnosis was possible in fractures of the radial, middle and ulnar carpal bone as

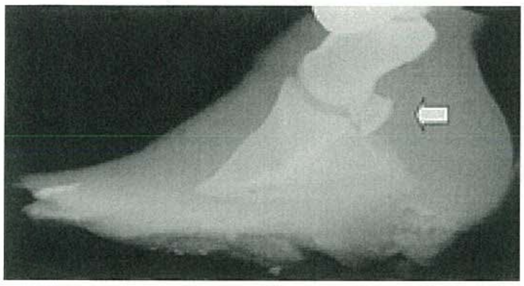

Fig. 3. An X-ray image of a hoof. Imaging conditions: 70 kV, 0.6 mAs. The arrow indicates the navicular bone.

Fig. 4. A 3D image of a hoof captured by MDCT visualizing details of the deep part of the hoof and the navicular bone. The arrow indicates the navicular bone. Imaging conditions: 120 kV, 150 mA, 0.5-mm slice thickness.

Fig. 5. An X-ray image of a comminuted fracture of the proximal phalanx. Multiple X-ray images are required to diagnose this type of fracture. Imaging conditions: 70 kV, 0.6 mAs.

Fig. 6. A 3D image captured by MDCT showing the comminuted fracture of the proximal phalanx. More precise interpretation is possible with a 3D image of the fracture. Imaging conditions: 120 kV, 150 mA, 1-mm slice thickness.

well as the 3rd and 4th carpal bones (Fig. 8). For the head images, the sinus paranasales was captured using the virtual endoscopic function of the software. We used a path from the left nostril to the sinus paranasales via the nasal meatus (Fig. 9). The sinus paranasales was captured by going up the ethmoid of the turbinated bone through the frontomaxillary opening to the frontal sinus. In the swayback case, X-ray image of the cervical vertebrae visualized stenosis and a ski jump of the spinal canal between the 5th and 6th cervical

Fig. 7. An X-ray image of a comminuted fracture of the left carpal bone. X-ray images need to be taken from various angles in order to identify a fracture in the carpal bone. Imaging conditions: 70 kV, 0.6 mAs.

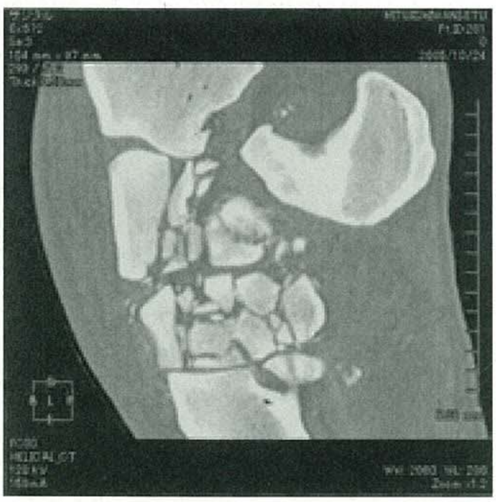

Fig. 8. An MDCT image of a comminuted fracture of the left carpal bone (the sagittal section of the lateral carpopodite). Comminuted fractures of the middle carpal bone and the 4th carpal bone were clearly captured. Imaging conditions: 120 kV, 150 mA, 0.5 mm slice thickness.

vertebrae (Fig. 10). In MDCT images, however, multiple sagittal sections visualized the stenosis of the spinal canal between the 5th and 6th cervical vertebrae (Fig. 11) and virtual endoscopic images visualized the stenosis as well as the ski jump when compared to

Fig. 9. The sinus paranasales constructed by the virtual endoscopic function of MDCT. The white arrow indicates the frontomaxillary opening. The black arrow indicates the frontal sinus. Imaging conditions: 135 kV, 150 mA, 2 mm slice thickness.

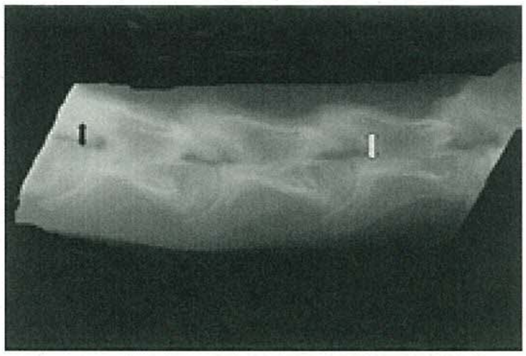

Fig. 10. An X-ray image of the cervical vertebrae of the swayback horse. Right to left: the 2nd, 3rd, 4th, 5th and 6th cervical vertebrae. Ski jump and stenosis of the spinal canal are evident between the 5th and 6th cervical vertebrae when compared with normal vertebrae. Imaging conditions: 70 kV, 0.6 mAs.

normal vertebrae (Fig. 12).

CT units are designed for human medical use, so that a trestle is needed for their application to large animals. In this study, MDCT was able to capture images of a generally anesthetized horse when a trestle for large animals was connected to a table for a human CT unit. Under general anesthesia, images we captured were limited to the carpopodite and hock or lower parts in

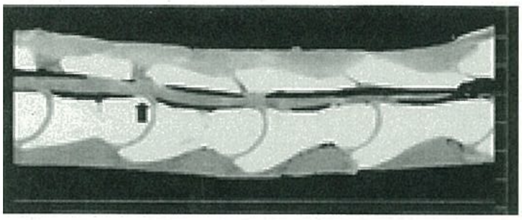

Fig. 11. A saggital image captured by MDCT, showing the cervical vertebrae of the swayback horse. Right to left: the 3rd, 4th, 5th and 6th cervical vertebrae. Multiple images of sagittal sections indicated the stenosis between the 5th and 6th cervical vertebrae. The arrow indicates the stenosis. Imaging conditions: 120 kV, 150 mA, 1 mm slice thickness.

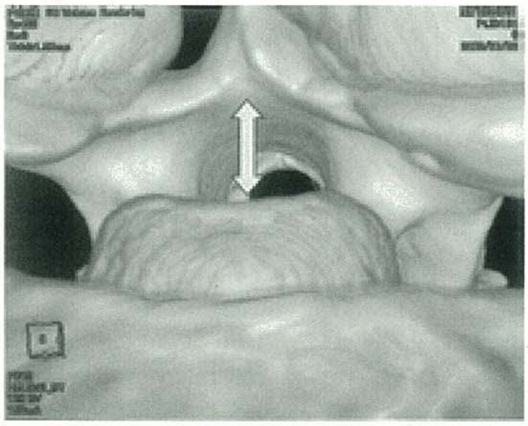

Fig. 12. An MDCT image of the cervical vertebrae of the swayback horse taken from the virtual endoscope. The arrow shows a stenosis of the spinal canal, between the 5th and 6th cervical vertebrae. Imaging conditions: 120 kV, 150 mA, 1 mm slice thickness.

the forelimb and hindlimb. This restriction was associated with the trestle having a limited movable range. Images of more proximal sites could be captured by widening the movable range and changing the height of the trestle.

MDCT images of the hoof clearly visualized the deep part, especially the navicular bone. Conventionally, diseases in the deep part of the hoof, such as navicular disease, have been diagnosed by plain X-ray and ultrasound examination [2, 8]. It has been difficult to obtain an image clear enough to make a diagnosis because lesions are covered with other tissues. However, MDCT is considered effective for making detailed diagnosis of bone lesions, such as navicular inflammation, since it can create detailed 3D reconstructed images of the navicular bone and the surrounding structure from a cross, horizontal, and/or sagittal angles. X-ray images of comminuted and multiple fractures are not always clear, and a detailed interpretation is said to require images from multiple angles [4]. In this study, however, 3D constructed images and cross-sectional images in MDCT visually helped us to understand helical fracture lines and carpal bone fractures in details. Possible use of MDCT was suggested in determination of the correct site for arthroscopic surgery and screw fixation procedures as well as for postoperative assessment.

The virtual endoscopic function in an image processing workstation enabled us to approach the sinus paranasales. The virtual endoscope visualized from the nostrils to the guttural pouch and sinus paranasales in a computer as if a real endoscopic observation had been. Thus, other than sinusitis, MDCT may be used for diagnosis of diseases such as guttural pouch infection. The supine position was preferable for problems in the head, and more stable operation may be possible by installing a head restraint on the table. Conventionally, plain X-ray, 2D images are used in diagnosis of swayback [7, 9, 10], but identification of stenosis has been difficult in some cases. Since MDCT collects volume data every few millimete, images with less partial volume effect can be captured, and higher precision is expected in determination of stenosis of the cervical spinal canal. Virtual endoscopic images that showed the 3D vertebral canal led to visual diagnosis of stenosis (Fig. 12), and suggested the usefulness of MDCT in a swayback diagnosis. We plan to further assess the usefulness of MDCT using a higher number of swayback cases and by comparing MDCT images with plain X-ray images.

Further clinical assessment of MDCT as a diagnosis tool could improve diagnosis in live animals. The application of MDCT to the fracture of the limbs, head and neck trouble, and thoracic disease and acute abdomen of foals is expected in the future. Accordingly, it will be necessary to examine the application of CT imaging with iodine contrast agent, as well as determining standard criteria for image assessment. In conclusion, MDCT wais considered effective for diagnosing fractures, diseases in the sinus paranasales and wobbler syndrome, the diagnoses of which have been difficult with plain X-ray images.

References

1. Barber, S.M. 2005. Management of neck and head injuries. *Vet. Clin. North. Am. Equine. Pract.* **21**: 191–215.
2. Dyson, S., Murray, R., Schramme, M., and Branch, M. 2003. Lameness in 46 horses associated with deep digital flexor tendonitis in the digit: diagnosis confirmed with magnetic resonance imaging. *Equine Vet. J.* **35**: 681–690.
3. Kopp, A.F., Heuschmid, M., and Claussen, C.D. 2002. Multidetector helical CT of the liver for tumor detection and characterization. *Eur. Radiol.* **12**: 745–752.
4. Kraus, B.M., Richardson, D.W., Nunamaker, D.M., and Ross, M.W. 2004. Management of comminuted fractures of the proximal phalanx in horses: 64 cases (1983–2001). *J. Am. Vet. Med. Assoc.* **15**: 254–263.
5. Lepage, O.M., and Piccot-Crezollet, C. 2005. Transarterial coil embolisation in 31 horses (1999–2002) with guttural pouch mycosis: a 2-year follow-up. *Equine Vet. J.* **37**: 430–434.
6. Newton, J.R., Verheyen, K., Talbot, N.C., Timoney, J.F., Wood, J.L., Lakhani, K.H., and Chanter, N. 2000. Control of strangles outbreaks by isolation of guttural pouch carriers identified using PCR and culture of Streptococcus equi. *Equine Vet. J.* **32**: 515–526.
7. Spaul, G., and Palmer, A.C. 1980. Wobbler syndrome (cervical stenosis) in a Percheron colt. *Vet. Rec.* **107**: 362.
8. Stashak, T.S. Equine radiology. pp.176–186. *In*: Lameness. Adams Lameness in Horses, 4th ed. (Stashak, T.S. ed.), Lea & Febiger, Philadelphia.
9. Van Biervliet, J., Scrivani, P.V., Divers, T.J., Erb, H.N., de Lahunta, A., and Nixon, A. 2004. Evaluation of decision criteria for detection of spinal cord compression based on cervical myelography in horses: 38 cases (1981–2001). *Equine Vet. J.* **36**: 14–20.
10. Walmsley, J.P. 2005. Surgical treatment of cervical spinal cord compression in horses: A European experience. *Equine Vet. Edu.* **17**: 39–43.
11. Whitton, R.C., Buckley, C., Donovan, T., Wales, A.D., and Dennis, R. 1998. The diagnosis of lameness associated with distal limb pathology in a horse: a comparison of radiography, computed tomography and magnetic resonance imaging. *Vet. J.* **155**: 221–222.